J Mater Sci (2008) 43:5679–5684
DOI 10.1007/s10853-008-2798-4

INTERFACE SCIENCE

Structure and polytypic faults in $Ba_4NdMn_3O_{12}$ compound

H. Yang · Z. E. Cao · X. Shen · W. J. Feng · J. L. Jiang · J. F. Dai · R. C. Yu

Received: 14 March 2008 / Accepted: 9 June 2008 / Published online: 8 July 2008
© Springer Science+Business Media, LLC 2008

Abstract We have studied the structure and polytypic defect formation in the 12R perovskite-type $Ba_4NdMn_3O_{12}$ compound. Its structure was characterized using transmission electron microscopy (TEM). Like in the 12R ordered oxides of $Ba_4CeMn_3O_{12}$ and $Ba_4PrMn_3O_{12}$ (Fuentes et al., J. Solid State Chem. 177 (2004) 714), a cationic ordering between Nd and Mn is also expected to be established in $Ba_4NdMn_3O_{12}$ with the Nd ions located in the corner-sharing octahedra and the Mn ions located in the face-sharing octahedra. We also observed in the $Ba_4NdMn_3O_{12}$ phase two types of polytypic faults, i.e., the extrinsic hexagonal-type fault with the stacking sequence …*cchhhcc*… and the extrinsic cubic-type fault with the stacking sequence …*hhccchh*….

Introduction

The perovskite-based oxides with the general formula ABO_3 have been the focus of much research in the past two decades because of their intriguing structural and physicochemical properties. Structurally ABO_3 related perovskites can be described on the basis of close packed AO_3 layers (an AO_3 hexagonal layer is schematically shown in Fig. 1a) with B cations sandwiched between AO_3 layers to form BO_6 octahedra. The stacking sequence of the AO_3 hexagonal layers can be cubic, hexagonal, or a combination of both. The cubic close packing (*ccp*, or shortly *c*) of the AO_3 layers with the ABC stacking sequence leads to the perovskite structure in which all BO_6 octahedra share corners (see Fig. 1b) like in $SrTiO_3$. The hexagonal close packing (*hcp*, or shortly *h*) of the AO_3 layers with the AB stacking sequence forms arrays of face-sharing BO_6 octahedra along the [001] crystallographic axis (see Fig. 1c), for example $BaNiO_3$. An association of mixed cubic (*c*) and hexagonal (*h*) stacking sequences, depending on many factors, such as the synthesis conditions, cationic sizes, electronegativity, and valence of the elements, allows one to generate an unlimited number of perovskite-based polytypes containing both corner- and face-sharing BO_6 octahedra. Furthermore the introduction of oxygen-deficient $AO_{3-\delta}$ layers adds an additional number of varieties.

Stoichiometric $BaMnO_3$ crystallizes in the 2H perovskite-based structure [1]; however, introducing oxygen deficiency into its framework leads to a mixed cubic and hexagonal packing of $BaO_{2.5}$ and BaO_3 layers, resulting in a series of $BaMnO_{3-\delta}$ varieties (21R-, 15R-, 8H-, 6H-, 10H-, 4H-type structures) [2–6]. It has also been established that the replacement of Mn by a cation of different size and of different valence is susceptible to generate new hexagonal-type structure derivatives, for example, 6H-$Ba_3ErMn_2O_9$ [7], 9R-($Ba_3MnRu_2O_9$, $Ba_9Ru_{3.2}Mn_{5.8}O_{27}$) [8, 9], 12R-($BaTi_{0.5}Mn_{0.5}O_3$, $Ba_4CeMn_3O_{12}$, $Ba_4PrMn_3O_{12}$, $Ba_{12}Ca_3Mo_3Mn_6O_{36}$, $Ba_{12}In_3Mn_9O_{34.5}$) [10–12], 12H-$Ba_6Ru_2Na_2Mn_2O_{17}$ [13], 15R-$Ba_5MnNa_2V_2O_{13}$ [14], 16H-$Ba_4Ca_{0.9}Mn_{3.1}O_{11.3}$ [15], 21R-$Ba_7Ca_2Mn_5O_{20}$ [16]. For most of the

H. Yang (✉)
State Key Laboratory of Gansu Advanced Non-ferrous Metal Materials, Lanzhou University of Technology, Lanzhou 730050, People's Republic of China
e-mail: hyang@lut.cn

H. Yang · Z. E. Cao · X. Shen · W. J. Feng · J. L. Jiang · J. F. Dai
School of Science, Lanzhou University of Technology, Lanzhou 730050, People's Republic of China

R. C. Yu
Beijing National Laboratory for Condensed Matter Physics, Institute of Physics, Beijing 100080, People's Republic of China

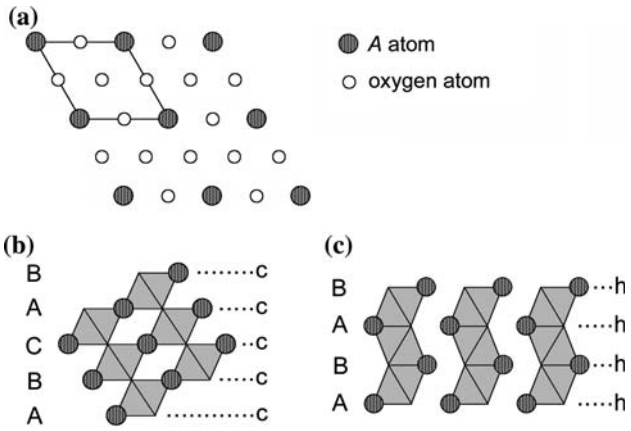

Fig. 1 (**a**) Representation of a hexagonal AO_3 layer. (**b**) Pure cubic close packing of AO_3 layers, leading to a 3C-type perovskite with the stacking sequence *ccc*. (**c**) Pure hexagonal close packing of AO_3 layers, leading to a 2H-type perovskite with the stacking sequence *hh*

Mn-site substituted derivatives, a remarkable cationic ordering, which is usually regarded to be one of the factors (other factors include oxygen content, Mn valency, cationic size, etc.) for the originality and stabilization of numerous perovskite-based polytypes, has been shown in their structures. For example, in the 12R-type $Ba_4REMn_3O_{12}$ (RE = Ce, Pr) structure [11] as shown in Fig. 2, the *RE* cations are located in the corner-sharing octahedra, whereas the Mn cations occupy the face-sharing octahedra, leading

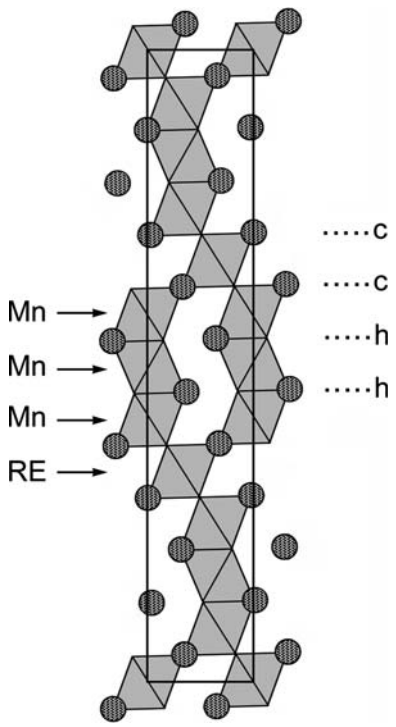

Fig. 2 [100] projection of the structure of $Ba_4REMn_3O_{12}$ (RE = Ce, Pr) (12R-type structure) [11]

to a cationic ordering between *RE* and Mn. In terms of the cationic ordering, by adequately changing the stoichiometry of composition (cationic ratio) and adjusting the thermodynamic conditions it is expected to form a sequence of perovskite polytypes. Generally, one or two of the expected polytypes are favorably stabilized in a given doped system. For example, the substitutions of Mn by Ce and Pr in $BaMnO_{3-\delta}$ lead to the favorable stability of 12R perovskite polytypes with the formula $Ba_4CeMn_3O_{12}$ and $Ba_4PrMn_3O_{12}$ [11]. Studies on the Ce and Pr doped systems with a cationic composition (a Ce/Mn ratio, or a Pr/Mn ratio) deviating from 1:3 have suggested that intergrowth structures instead of a single-phase polytype were formed in the examined composition [11]. In the case of the Er substitution, it has been shown that the formation of a 6H perovskite polytype with composition $Ba_3ErMn_2O_9$ is favored [7].

In this work we present a transmission electron microscopy (TEM) study of the crystal structure and polytypic faults in the $Ba_4NdMn_3O_{12}$ compound.

Experimental

Polycrystalline sample of $Ba_4NdMn_3O_{12}$ was synthesized by the standard oxide ceramic processing technique. A stoichiometric mixture of Nd_2O_3, $BaCO_3$, and $MnCO_3$ powders was well ground and calcined twice at 800 and 950 °C for 24 h. Then, the resulting powders were pressed into pellets and sintered at 1,300 °C for 12 h. The phase purity was examined by means of powder X-ray diffraction (XRD) using Cu Kα radiation. The samples for electron diffraction (ED) and high-resolution transmission electron microscopy (HRTEM) studies were prepared by crushing $Ba_4NdMn_3O_{12}$ ceramic in an agate mortar filled with alcohol, and then dispersing the fine fragments suspended in alcohol on a holey carbon film supported by a copper grid. A Tecnai F20 field-emission transmission electron microscope, operated at an acceleration voltage of 200 keV, was used for the TEM studies. Image simulations were carried out using the multi-slice algorithm of dynamical scattering [17].

Results and discussion

Figure 3 shows the XRD pattern for the $Ba_4NdMn_3O_{12}$ sample, which is very similar to those of the 12R perovskite-type manganites reported in the literature [11, 12], indicating that $Ba_4NdMn_3O_{12}$ crystallizes in the 12R-type structure. This structure is further reinforced by the resultant ED and high-resolution TEM data. Figure 4 shows the ED patterns recorded along the [001] and [100] zone-axis directions. The systematic extinction conditions, observed

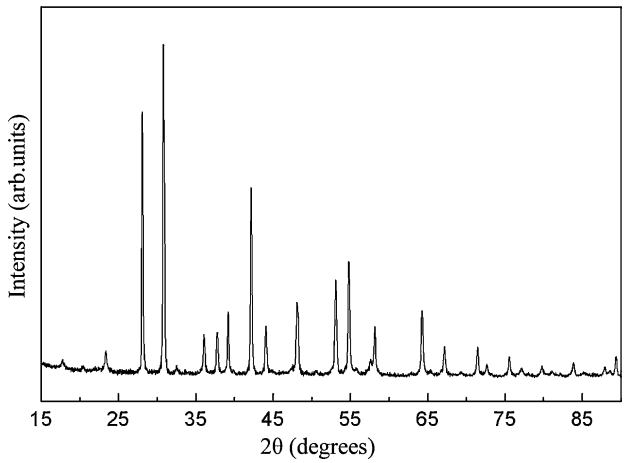

Fig. 3 Powder X-ray diffraction pattern for $Ba_4NdMn_3O_{12}$

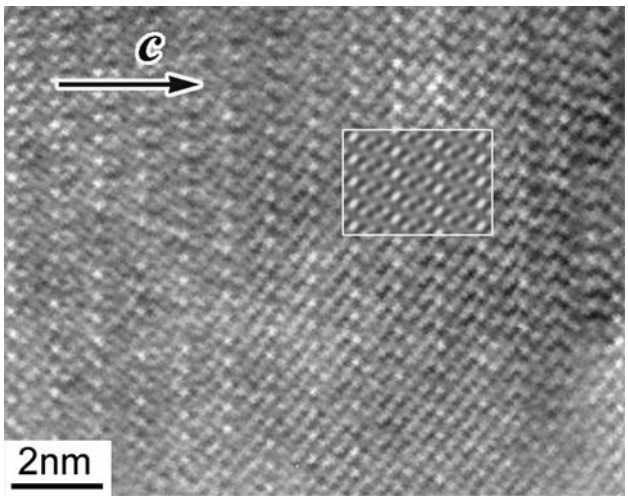

Fig. 5 HRTEM image of $Ba_4NdMn_3O_{12}$ taken along the [100] direction. A simulated image (thickness: 2.3 nm, defocus value: −70 nm) is embedded on the experimental image to produce the good agreement

to be $-h + k + l = 3n$ in general, $-h + l = 3n$ for $(h0l)$ and $l = 3n$ for $(00l)$, are compatible with the space group $R\,\bar{3}\,m$ (166). The camera length was calibrated using TlCl, and the lattice parameters were derived from the ED patterns as: $a = 0.58$ nm and $c = 2.86$ nm. Figure 5 shows a HRTEM image taken along the [100] zone-axis direction. This image was obtained from a thin region of the crystal under the defocus value of ~ -70 nm. Assuming that the $Ba_4NdMn_3O_{12}$ phase is isostructural with $Ba_4PrMn_3O_{12}$, its structure model can be derived approximately from that of the latter [11] since the atomic radius of Nd is very close to that of Pr. A simulated image for a crystal thickness of 2.3 nm and a defocus value of −70 nm, superimposed onto the image, fits perfectly with the experimental, further confirming that the $Ba_4NdMn_3O_{12}$ phase has a 12R-type perovskite structure. Like in the 12R ordered oxides of $Ba_{12}In_3Mn_9O_{34.5}$, $Ba_4CeMn_3O_{12}$, and $Ba_4PrMn_3O_{12}$, a cationic ordering between neodymium and manganese is also established in $Ba_4NdMn_3O_{12}$ with the Nd ions located in the corner-sharing octahedra and the Mn ions located in the face-sharing octahedra.

The composition analysis for the phase using TEM-EDX showed that the actual cationic ratio is close to the nominal one, indicating no vacancies in the cationic sites. Generally, the oxygen content is difficult to determine precisely by EDX. As the common oxidation state of neodymium in the perovskite oxides is Nd^{3+} state, the oxygen deficiency possibly exists in the $Ba_4NdMn_3O_{12}$ compound according to the requirement of electroneutrality. We also prepared the samples of other cationic compositions (Nd/Mn ratio) in the Ba–Nd–Mn–O system; however, no single-phase samples were obtained. For example, an attempt to prepare $Ba_3NdMn_2O_9$ resulted in the coexistence of the perfect 12R-type structure with an average chemical composition of $Ba_4NdMn_3O_{12}$ and the

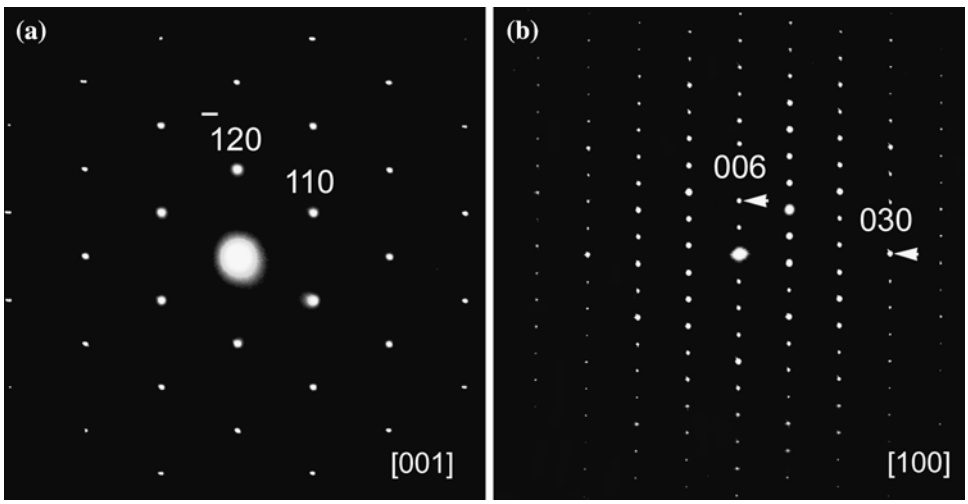

Fig. 4 ED patterns of $Ba_4NdMn_3O_{12}$ taken along the (**a**) [001] and (**b**) [100] zone-axis directions

Nd rich modulated superstructure [18]. These results indicate that for the Ba–Nd–Mn–O system the formation of perfect 12R polytype requires the composition to be $Ba_4NdMn_3O_{12}$, and this composition is just the requirement, from a stoichiometric point of view, for the cationic ordering between Nd and Mn in this polytype. This also suggests that the cationic ordering plays an important role for the stabilization of the 12R-type structure. Previous studies have suggested that the substitution of A-sites (i.e. Ba-sites) by Nd in the $BaMnO_{3-\delta}$ system leads to a 3C-type perovskite [19].

In the 12R $Ba_4NdMn_3O_{12}$ phase, we observed two types of polytypic planar faults. One of them can be characterized as the extrinsic hexagonal-type fault (EHF). Figure 6 shows an ED pattern of a crystal fragment containing the EHF. One can see that this ED pattern consists of two sets of diffraction spots, which can be separately indexed on the [100] and $[\bar{1}00]_T$ zone axes, as schematically demonstrated on the right in Fig. 6. The relationship between the two sets of diffraction spots reveals a twined structure resulting from the EHF. High-resolution transmission electron microscopy was also used to investigate the faults. Figure 7 shows a [100] zone-axis HRTEM image, revealing parallel planar faults of this type.

The formation of the EHF in the 12R-type perovskite can be explained in terms of the stacking sequence of BaO_3 close packed layers. The perfect 12R polytype is constructed from a …*cchhcc*… stacking sequence of BaO_3 layers. When the normal sequence is broken by inserting or removing BaO_3 layers, stacking defects are consequently formed in the 12R phase. The EHF, which can be regarded as one of the stacking defects, is formed by sandwiching an extra hexagonal BaO_3 layer in one of the hexagonal stacked blocks, as shown in Fig. 8. The resulting stacking sequence of close packed layers in the fault region is then described as …*cch*$\underline{h}$*hcc*…. Alternatively, removing an *h* layer from one of the hexagonal stacked blocks, consequently leading to the local stacking sequence changed to be …*cchcc*…, is also expected to result in a fault similar to EHF. The generation of the EHF can be also understood as the result of the replacement of a block with three face-sharing octahedra by a block with four (or two) face-sharing octahedra.

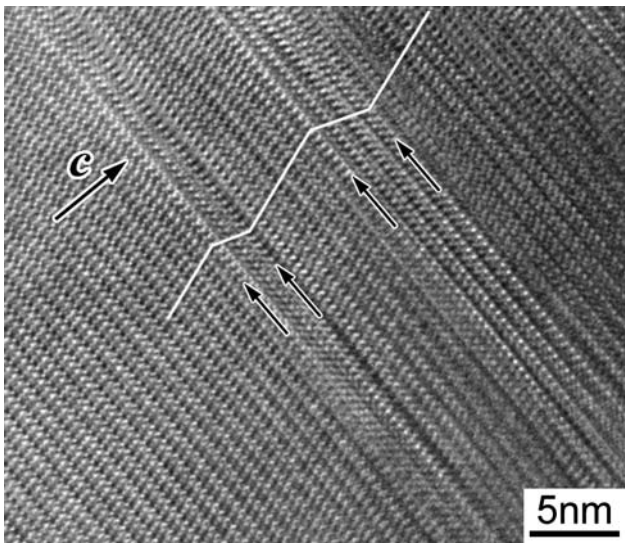

Fig. 7 A [100] zone-axis HRTEM image of $Ba_4NdMn_3O_{12}$, revealing parallel extrinsic hexagonal-type faults

The HRTEM image given in Fig. 9 reveals another type of polytypic planar fault as indicated by the arrow. One can see that the two grains across the fault are parallel to each other, and the boundary lies in a definite (001) plane with no lattice distortion in the interface. In fact, it is only with the atomic contrast that one can read out a fault in the image, indicating that the fault region still has a perfect close packed structure. This polytypic fault can be explained as the extrinsic cubic-type fault (ECF). Figure 10 shows a structure model of the ECF. According to the model, the polytypic fault is formed by inserting a cubic BaO_3 layer in one of the cubic stacked blocks, where the stacking sequence is then changed to be …*hhcc*$\underline{c}$*hh*….

It should be pointed out that to vary irregularly the stacking sequence of close packed layers in a perovskite-based oxide is expected to result in the complex intergrowth structures. The intergrowth faults were commonly

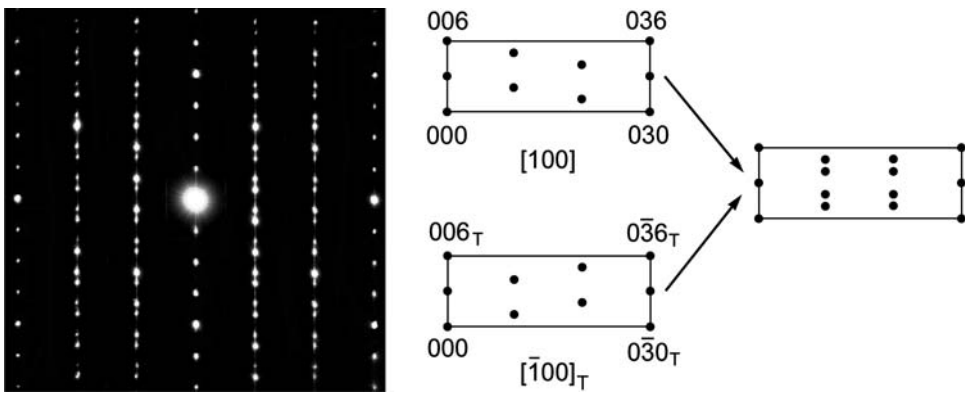

Fig. 6 ED pattern of a $Ba_4NdMn_3O_{12}$ crystal fragment, revealing a twined structure in the crystal. The two sets of diffraction spots in the ED pattern can be separately indexed on the [100] and $[\bar{1}00]_T$ zone axes, as schematically demonstrated on the right

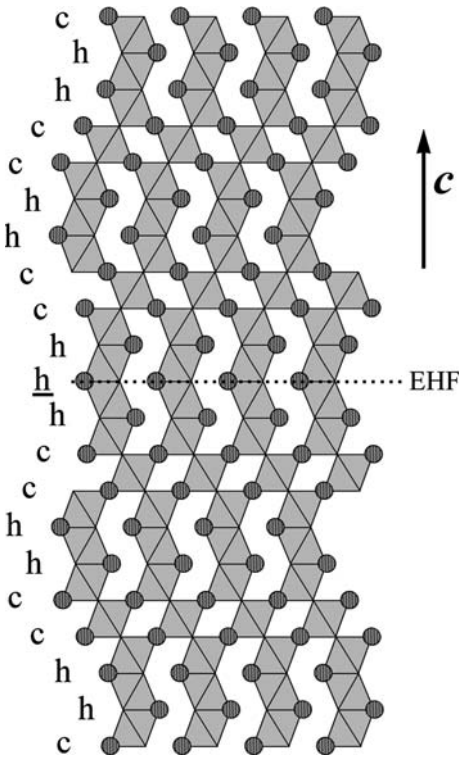

Fig. 8 Schematic [100] projection of the extrinsic hexagonal-type fault, which is formed by inserting an extra hexagonal BaO_3 layer in one of the hexagonal stacked blocks

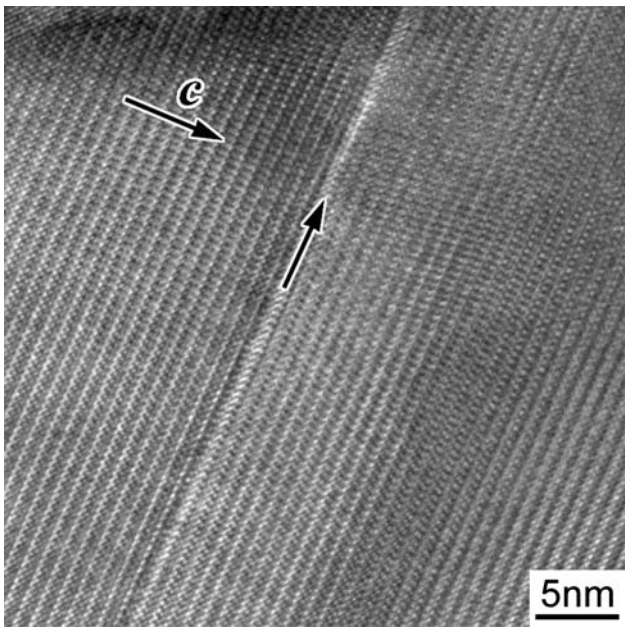

Fig. 9 A [100] zone-axis HRTEM image of $Ba_4NdMn_3O_{12}$, showing an extrinsic cubic-type fault

found in the multilayer ABO_3 perovskites (for example, $BaMnO_{3-\delta}$ [20] and $Ba_5CeMn_4O_{15}$ [11]), as well as in the two-dimensional layered perovskites with the general

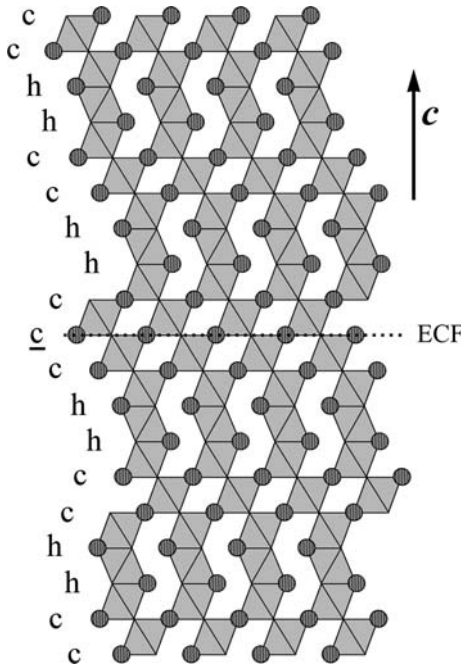

Fig. 10 A structure model of the extrinsic cubic-type fault. The fault is formed by inserting a cubic BaO_3 layer in one of the cubic stacked blocks

formula $A_{n+1}B_nO_{3n+1}$ (for example, $La_xCa_{4-x}Mn_3O_{10}$ [21] and $Ba_6Mn_5O_{16}$ [22]).

Conclusions

By substitution of Mn by Nd on the B-sites in the hexagonal $BaMnO_3$ compound, we have isolated a 12R perovskite-type manganite with a nominal composition of $Ba_4NdMn_3O_{12}$. Based on stoichiometric and structural similarity with related compounds [11], we suggest that in the 12R $Ba_4NdMn_3O_{12}$ phase, the Nd ions are located in the corner-sharing octahedra while the Mn ions sit in the face-sharing octahedra, leading to a cationic ordering between Nd and Mn. Two types of polytypic faults, resulting from the local changes of stacking sequences of the AO_3 close packed layers, were revealed in the $Ba_4NdMn_3O_{12}$ phase. To our knowledge, there are few reports of such boundary-like faults in multilayer perovskites constructed from mixed cubic/hexagonal stacking sequences.

Acknowledgements This work was supported by the Foundation of Gansu Educational Committee (0703B-01), the Doctoral Research Grant of Lanzhou University of Technology (SB10200701), the Natural Science Foundation of Gansu Province (Grant Nos. ZS032-B25-019 and 3ZS061-A25-039), and State Key Laboratory of Gansu Advanced Non-ferrous Metal Materials (Grant Nos. SKL07003 and SKL05009). R. C. Yu thanks the National Natural Science Foundation of China (Grant Nos. 10774168 and 50621061) and the State Key Development Program for Basic Research of China (Grant Nos. 2005CB623602 and 2007CB925003) for the support.

References

1. Cussen EJ, Battle PD (2000) Chem Mater 12:831. doi:10.1021/cm991144j
2. Negas T, Roth RS (1971) J Solid State Chem 3:323. doi:10.1016/0022-4596(71)90068-5
3. Parras M, Alonso J, González-Calbet JM, Vallet-Regi M (1993) Solid State Ionics 63–65:614. doi:10.1016/0167-2738(93)90168-3
4. González-Calbet JM, Parras M, Alonso JM, Vallet-Regí M (1993) J Solid State Chem 106:99. doi:10.1006/jssc.1993.1268
5. Parras M, González-Calbet JM, Alonso J, Vallet-Regí M (1994) J Solid State Chem 113:78. doi:10.1006/jssc.1994.1344
6. Parras M, Alonso J, González-Calbet JM, Vallet-Regí M (1995) J Solid State Chem 117:21. doi:10.1006/jssc.1995.1241
7. Rabbow C, MullerBuschbaum H (1994) Z Naturforsch (B) 49:1277
8. Serpil Gö1nen Z, Gopalakrishnan J, Eichhorn BW, Greene RL (2001) Inorg Chem 40:4996
9. Frenzen S, MullerBuschbaum H (1994) Z Naturforsch (B) 50:585
10. Keith GM, Kirk CA, Sarma K, Alford NM, Cussen EJ, Rosseinsky MJ et al (2004) Chem Mater 16:2007. doi:10.1021/cm035317n
11. Fuentes AF, Boulahya K, Amador U (2004) J Solid State Chem 177:714. doi:10.1016/j.jssc.2003.08.025
12. Créon N, Michel C, Hervieu M, Maignan A, Raveau B (2003) Solid State Sci 5:243. doi:10.1016/S1293-2558(02)00098-5
13. Quarez E, Abraham F, Mentré O (2003) J Solid State Chem 176:137. doi:10.1016/S0022-4596(03)00379-7
14. Bendraoua A, Quarez E, Abraham F, Mentré O (2004) J Solid State Chem 177:1416. doi:10.1016/j.jssc.2003.11.022
15. Floros N, Michel C, Hervieu M, Raveau B (2000) Chem Mater 12:3197. doi:10.1021/cm000277y
16. Floros N, Michel C, Hervieu M, Raveau B (2002) J Solid State Chem 168:11. doi:10.1006/jssc.2002.9667
17. Cowley JM, Moodie AF (1957) Acta Crystallogr 10:609. doi:10.1107/S0365110X57002194
18. Yang H, Tang YK, Yao LD, Zhang W, Li QA, Li FY et al (2007) J Alloy Compd 432:283. doi:10.1016/j.jallcom.2006.05.117
19. Suarda E, Fauthb F, Martinc C, Maignanc A, Millanged F, Kellere L (2003) J Magn Magn Mater 264:221. doi:10.1016/S0304-8853(03)00209-9
20. González-Calbet JM, Parras M, Alonso J, Vallet-Regí M (1994) J Solid State Chem 111:202. doi:10.1006/jssc.1994.1218
21. Yao LD, Yang H, Zhang W, Li FY, Jin CQ, Yu RC (2006) J Appl Phys 100:023907. doi:10.1063/1.2218469
22. Yang H, Yang RF, Li QA, Li FY, Jin CQ, Yu RC (2006) J Phys Chem Solids 67:2365. doi:10.1016/j.jpcs.2006.06.010